LA-UR-18-31017
Approved for public release; distribution is unlimited.

Title: Resistively Heated Target Tests Using Helium Flow Loop

Author(s): Wass, Alexander Joseph
Woloshun, Keith Albert
Dale, Gregory E.
Dalmas, Dale Allen
Romero, Frank Patrick
Naranjo, Angela Carol
Aragonez, Robert J.
Kollarik, Nathan

Intended for: Report

Issued: 2018-11-20

Resistively Heated Target Tests Using Helium Flow Loop

Alexander Wass, Keith Woloshun, Gregory Dale, Dale Dalmas, Frank Romero, Angela Naranjo, Robert Aragonez, Nathan Kollarik

30 October 2018

Introduction

A helium flow and heat transfer experiment has been conducted using the helium flow loop facility at the Los Alamos National Laboratory. In order to replicate the helium cooled Mo-100 plant design disks during beam heating, an array of resistive heaters were placed within the helium flow loop, and cooled via helium. The resistively heated test piece is comprised of seven ceramic electric heaters with embedded thermocouples allowing temperature measurements of each heater. Computation fluid dynamic (CFD) simulations and analysis from theory are compared to the experiment results in order to have predictable capabilities for future experiments.

Two geometry configurations of the tubing before and after the heater housing are also tested. The plant design for the Mo-100 to Mo-99 targets requires sharp bends and geometry changes in the helium flow tube immediately before and after the target. An idealized fully developed flow configuration with straight entry and exit is tested and compared with an option that employs rectangular tubing to make a 90° bend at a radius consistent with and practical for the actual plant design.

Geometry

In these experiments, the Mo-99 plant design target disks and holder, which form rectangular helium flow channels, are replicated by rectangular heaters with embedded thermocouples available from Watlow. This heater is only slightly smaller than the 29 mm plant design Mo-100 disks, so data can be readily scaled to the actual geometry of the plant design. The heaters are 2.5 mm thick, and the anticipated plant design target will have disk thicknesses ranging from 0.5 to 4 mm. These heaters offer a readily available solution that is of acceptable geometric similarity to the plant design, has imbedded thermocouples for heat transfer measurement, and sufficient heat (967 W) and heat flux (77 W/cm^2) for good heat transfer measurement. The 7 heaters are mounted in a holder with 0.5 mm coolant gaps, based on past tests and analysis of target cooling with the new blower for the plant target. Figure 1 shows the heater housing and heater assembly, along with the bullnose inlet and outlet heater geometry. The heaters are inserted from the top of the housing and held in place by the heater assembly. The heaters are supported by a stainless steel base and cover, which is attached to two support rods welded to a 4.62 inch flange. One 10 pin Type K thermocouple feedthrough and one 20 pin AWG 20 power feedthrough are screwed into the flange. The inlet and outlet of the heater housing have internal dimensions of 0.906 x 0.860 inches.

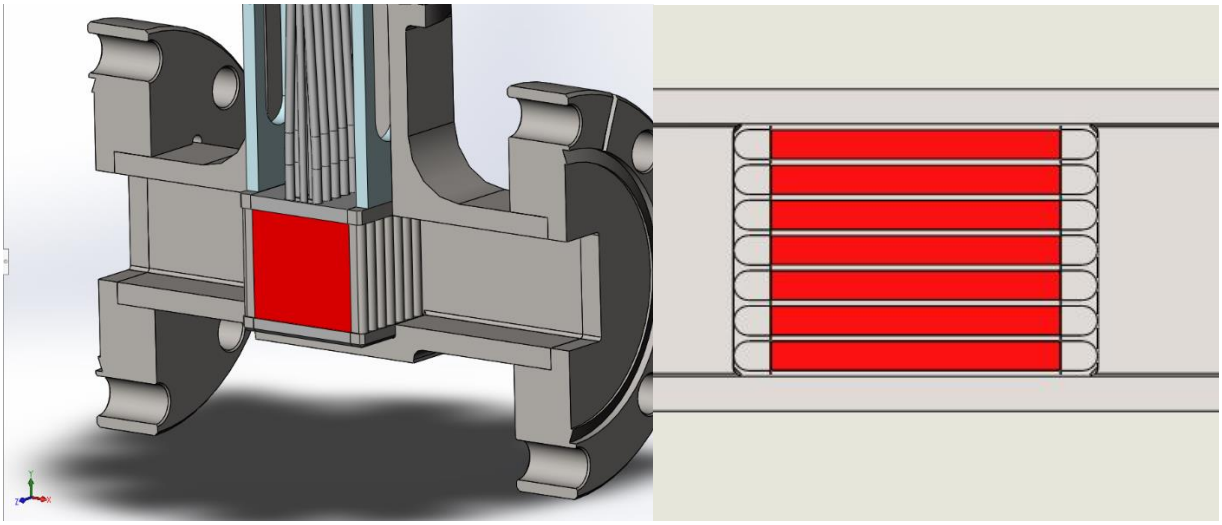

Figure 1 – Cut away view of heater housing with heaters (left) and top cross sectional view of heaters and flow channel features (right)

The first tubing configuration, shown in Fig. 2, shows the straight sections of 1.25 inch (outer dimension) square tubing as well as the heater housing. At the housing inlet (right), a 15 inch section of square tubing allows the flow of helium to become fully developed. The shorter, 10 inch section (left), connects to the return side of the flow loop. The second inlet and outlet tubing configuration contains two 90° bends at the inlet and outlet of the heater housing and is shown in Fig. 3. This tubing configuration matches more closely to the actual production plant design. The 90° rectangular bent tubes have a constant bend radius and internal dimensions of 0.906 x 0.858 inches. Before and after these bent tubes are a 2 inch schedule 40 pipe with a 90° bend at a constant radius.

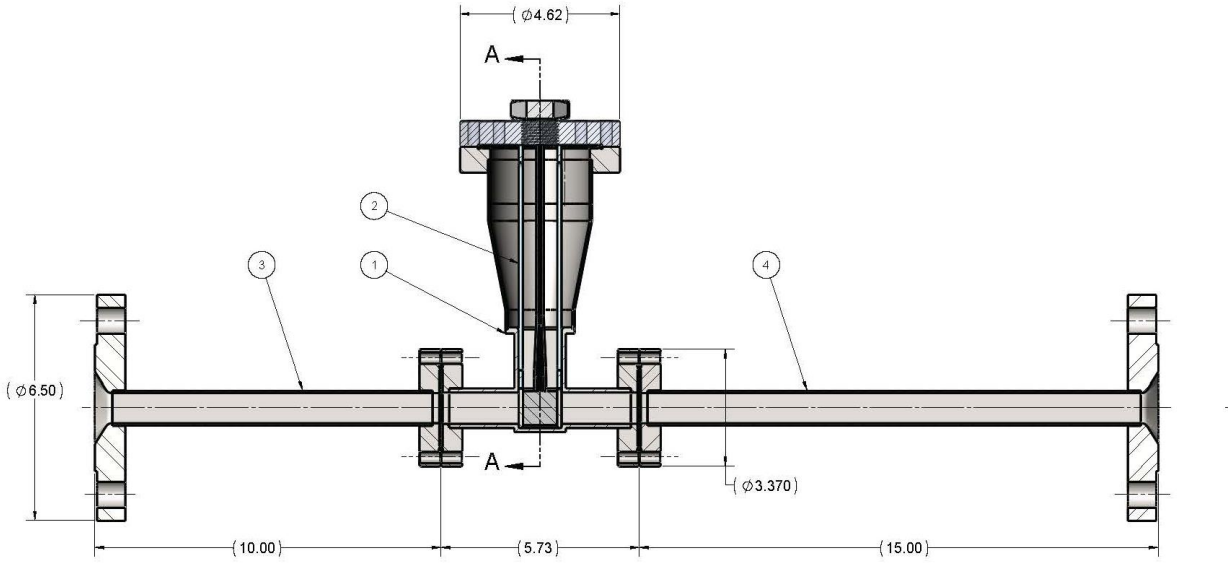

Figure 2 – Straight, rectangular tubing inlet and outlet for fully developed flow

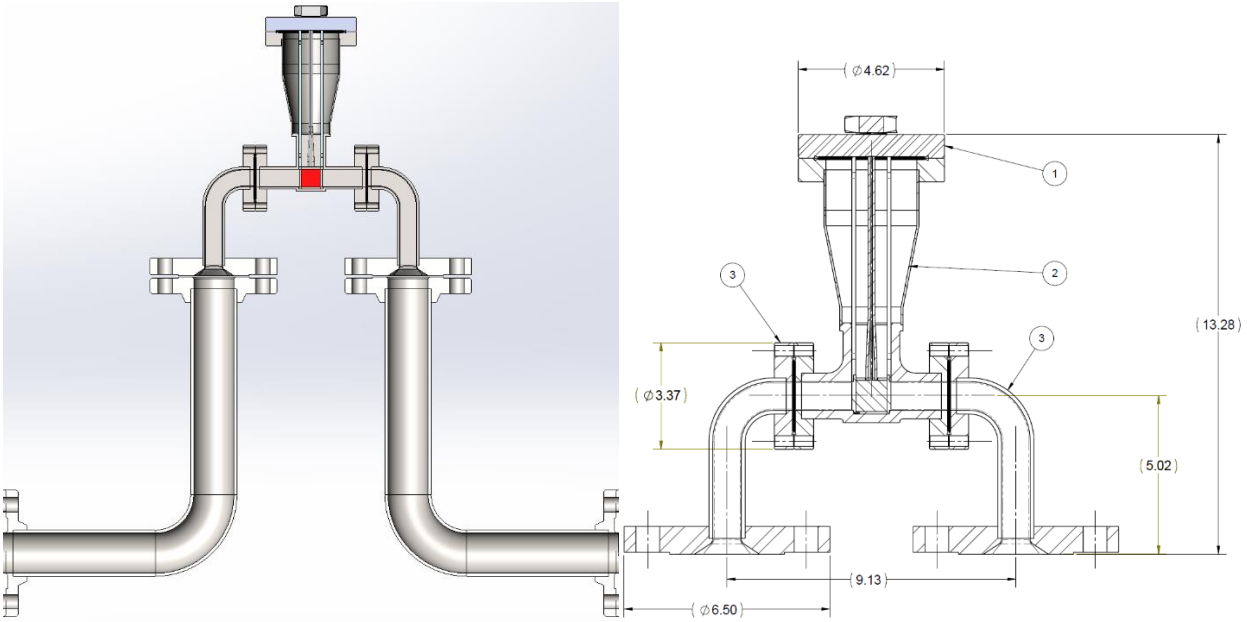

Figure 3 – 90° bent tubing configuration (left) and close-up cross section (right) similar to Mo-99 production plant design

Experiment

Setup and Instrumentation

The seven Watlow Ultramic 600 Advanced Ceramic resistive heaters were powered using a Sorenson 300-33T, 300 VDC and 33 A power supply, and later a Sorenson SGI330X30C, 330 VDC and 30A power supply. Since the appropriate outlet for the power supply was located across the room from the heater test section, about 200 feet of diesel locomotive eight gauge wire was ran from the power supply to the heater assembly. A power breakout box, which was custom built on site, was placed in-line in order to transfer power to the seven heaters. A schematic of the circuit can be seen in Appendix A. The circuit also provides means for determining individual heater voltage and current. Also, this circuit offers protection to the data acquisition modules in case of a current spike due to a loss in heater resistance.

Identical experiments were conducted using both tubing configurations shown in Figs. 4 and 5. Close-up pictures of the heater assembly can be seen in Figs. 6-10. A thermocouple was placed at the bottom of the heater housing to monitor wall temperature during heating. For additional safety controls, an interlock was added from the vortex flow meter to the power supply that shuts the supply off if the flow rate drops less than 20 g/s. Therefore, the heater power supply can only be turned on when there is sufficient flow. The helium flow rate was increased to 80 g/s (according to the turbine flow meter), and was decreased to 30 g/s in increments of 10 g/s. The temperature of the helium and heaters were allowed to stabilize before the flow rate was changed. The heaters were maintained at 236 V and up to 3.5 A per heater. Individual heater power was maintained between 750 and 800 W. The maximum power of the heaters (967 W) were not achieved due to the power losses in the long cable between the power supply and the heaters.

Figure 4 - Heater housing in line with the straight inlet and outlet configuration

Figure 5 - Heater housing in line with the 90° bend configuration with the power breakout box in the background

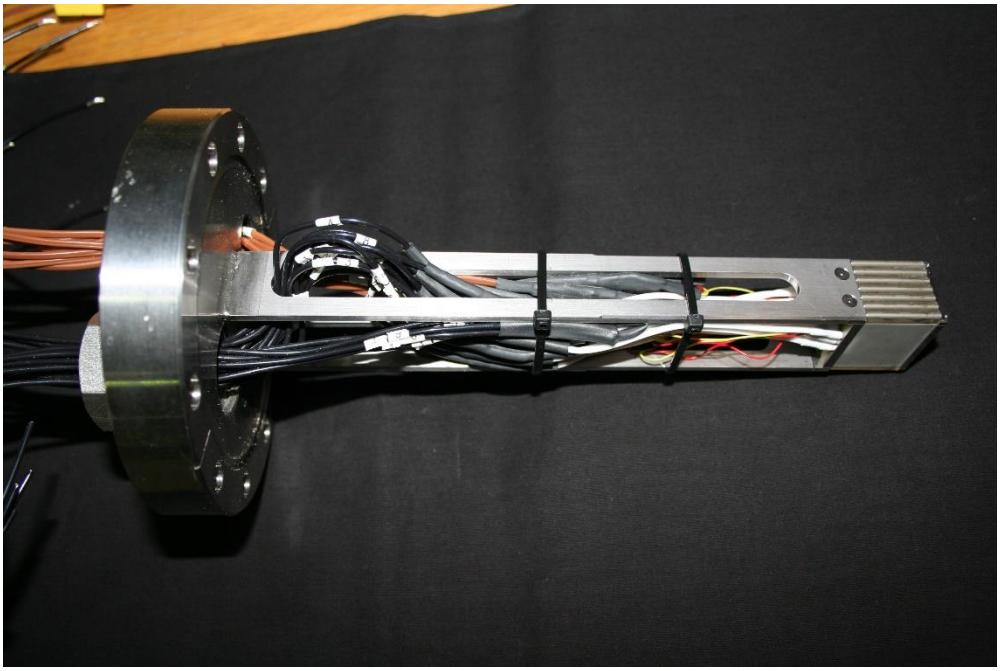

Figure 6 - Resistive heater assembly with attached power and thermocouple wires

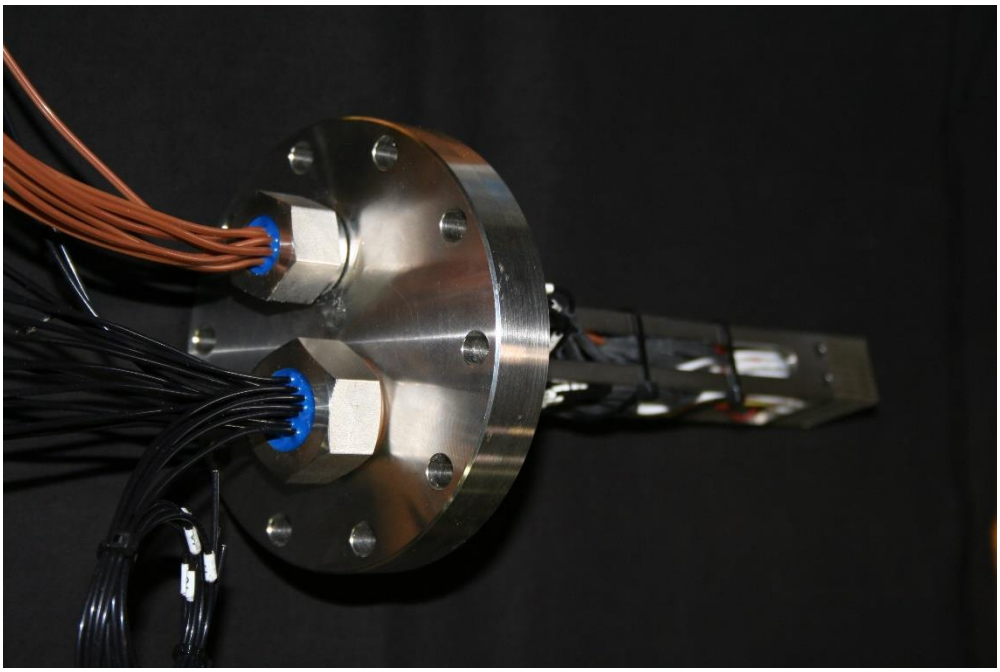

Figure 7 – Resistive heater assembly showing the power and thermocouple feedthroughs

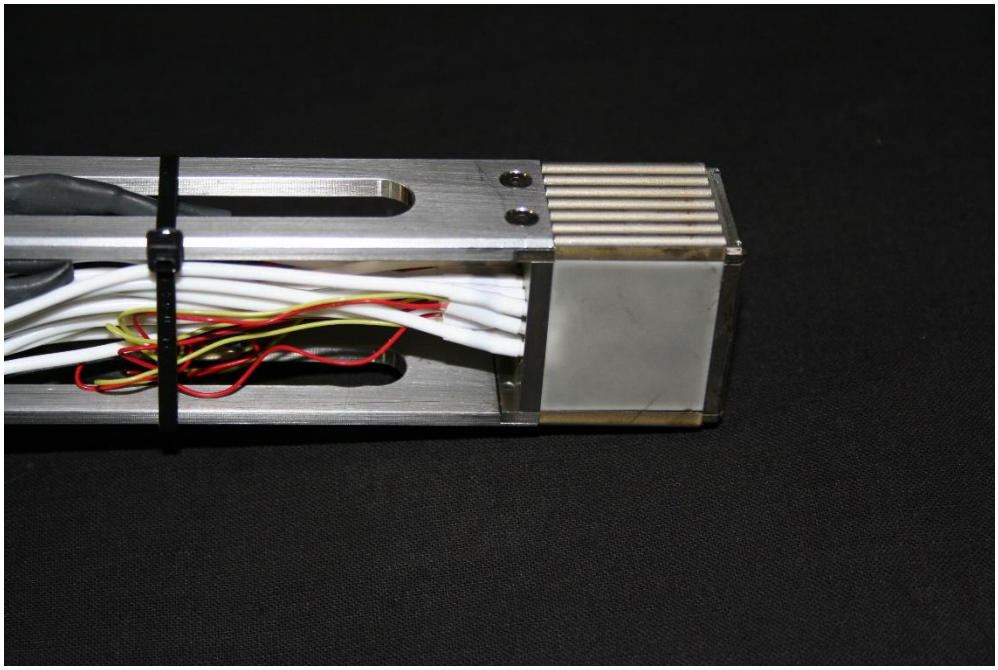

Figure 8 - Close-up view of the resistive heaters attached to the assembly

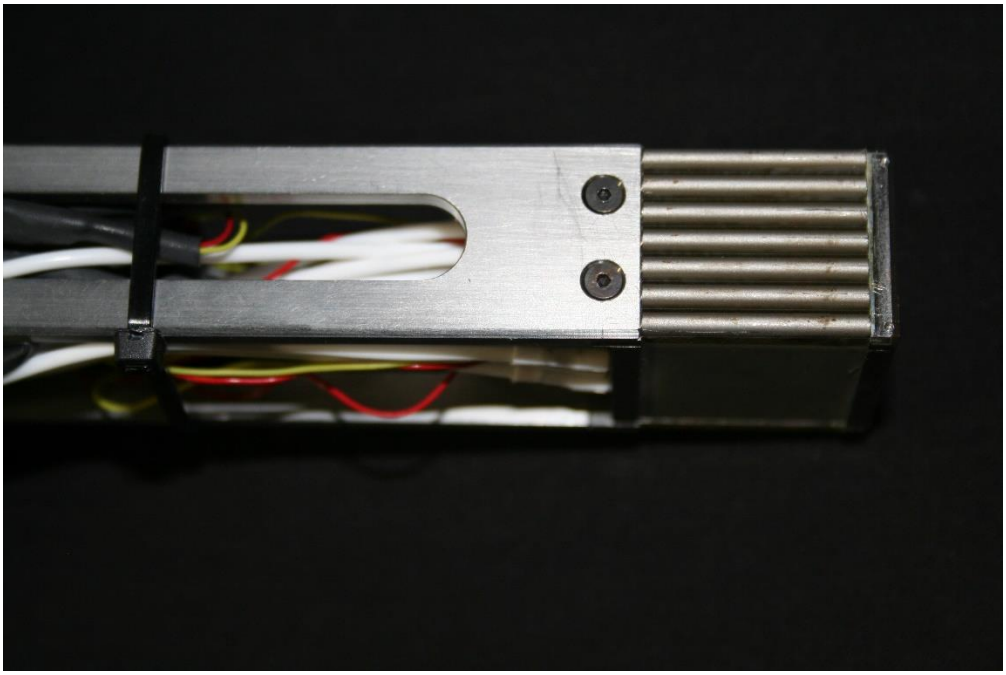

Figure 9 - Close-up view of the resistive heater assembly with bullnose geometry

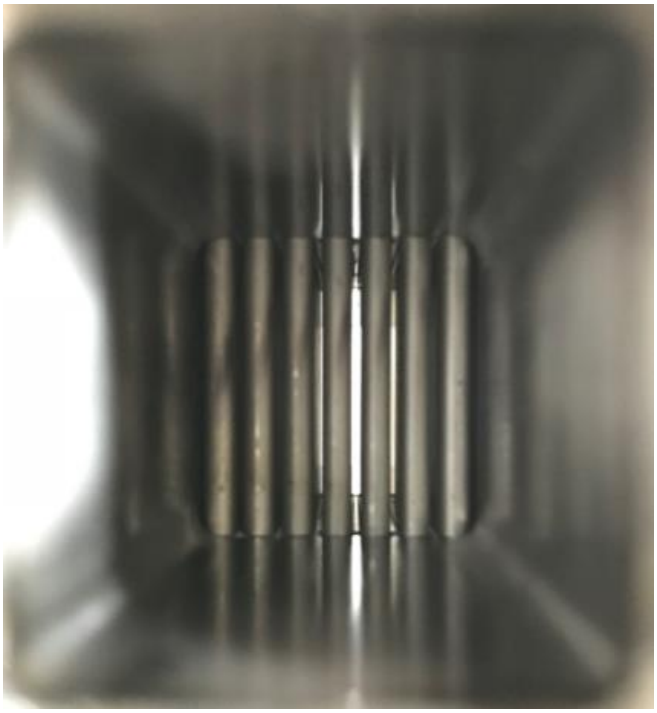

Figure 10 - Inlet view of the resistive heater array assembled in housing

Results

The inlet pressure was maintained between 320 and 340 psig with helium. Pressure drop during heating for both pipe configurations can be seen in Fig. 11. The pressure drop in the 90° bend configuration was slightly greater than in the straight, fully developed configuration since there is greater flow resistance in pipe elbows and bends such as in this experiment. Figure 12 shows the total heater and fluid power for both configurations. The fluid thermal power is calculated by $q_T = \dot{m} C_p \Delta T$, where $\dot{m}$ is mass flow rate, C_p is specific heat at constant pressure, and ΔT is the temperature difference between the inlet and outlet. One can see that the fluid power is greater than the heater power by up to 4%, which is a non-realistic result. The reason behind this could be due to inaccurate flow meter data. There are two flow meters in the flow loop. One operates on a vortex principle, and the other has a small turbine that rotates due to the flow. The vortex flow meter measured consistently lower than the turbine flow meter (8 g/s at max flow), however, the data in this report was recorded from the turbine flow meter which may slightly overestimate the mass flow rate. The actual flow rate is somewhere between the vortex and turbine flow meter outputs.

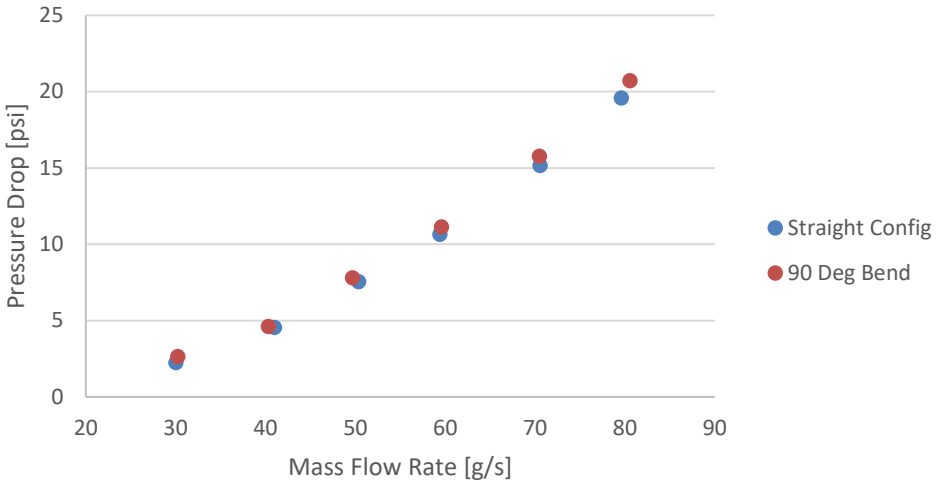

Figure 11 - Pressure drop for the straight inlet/outlet and 90° bend configurations during resistive heating

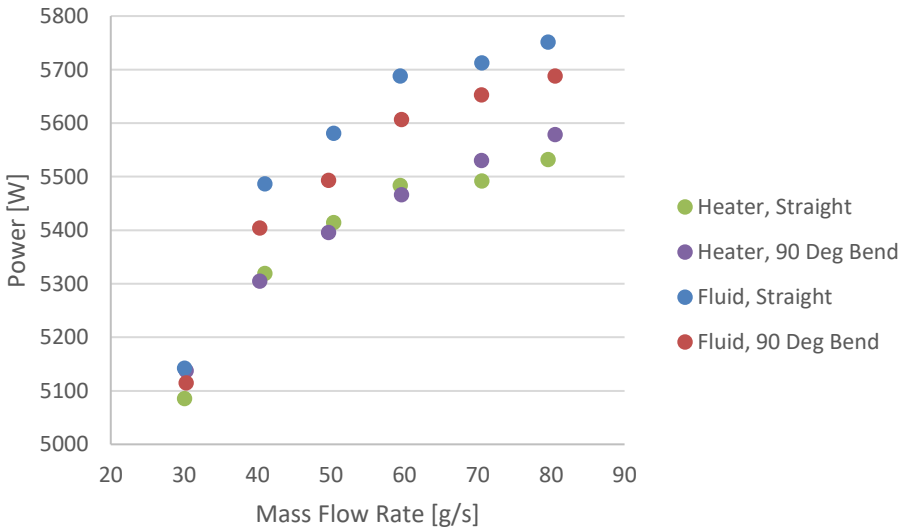

Figure 12 - Total heater power and fluid power for both configurations

The transient helium temperature at the inlet and outlet of the heaters can be seen in Figs. 13 and 14. The helium is cooled via water-cooled heat exchanger prior to the heater assembly inlet. The water returns to the facility evaporative cooling tower which has a single on/off thermostat. Therefore, the water temperature slowly increases temperature until a desired temperature is reached, and the cooling tower turns on, rapidly cooling the water. Thus, the helium inlet temperature also slowly rises until the water cooling tower turns on. This is clearly visible in the temperature plots. The cooling tower turned on in the middle of the first experiment with the straight configuration (Fig. 13). As a result, the heater temperatures decreased even as the helium flow rate also decreased.

The second experiment with the 90° bend configuration provided much better results since the water cooling tower remained off. Even though the fluid temperatures never reached steady state, the results are still valid since the slopes of the inlet and outlet temperatures are consistent. The scattered data around 3500 seconds for the straight configuration was due to the flow interlock with the power

supply. Initially, the flow interlock was set to 25 g/s, however, when approaching a flow rate of 30 g/s, the power supply shut off. After several attempts to operate at the desired flow rate, the interlock was lowered to 20 g/s and the power supply stayed on while maintaining a flow of 30 g/s. At the end of each experiment, the flow rate was increased back to 80 g/s to verify repeatability, hence the drop in temperature at the end. The temperature increase of the helium due to the heaters is shown in Fig. 15. The maximum temperature increase was 33°C at a flow rate of 30 g/s, and the lowest was about 13.5°C at 80 g/s. Slight variations in flow rate for the two configurations caused slight temperature variations as well. The heater housing bottom wall temperature remained cool for all of the flow rates and never exceeded 31°C.

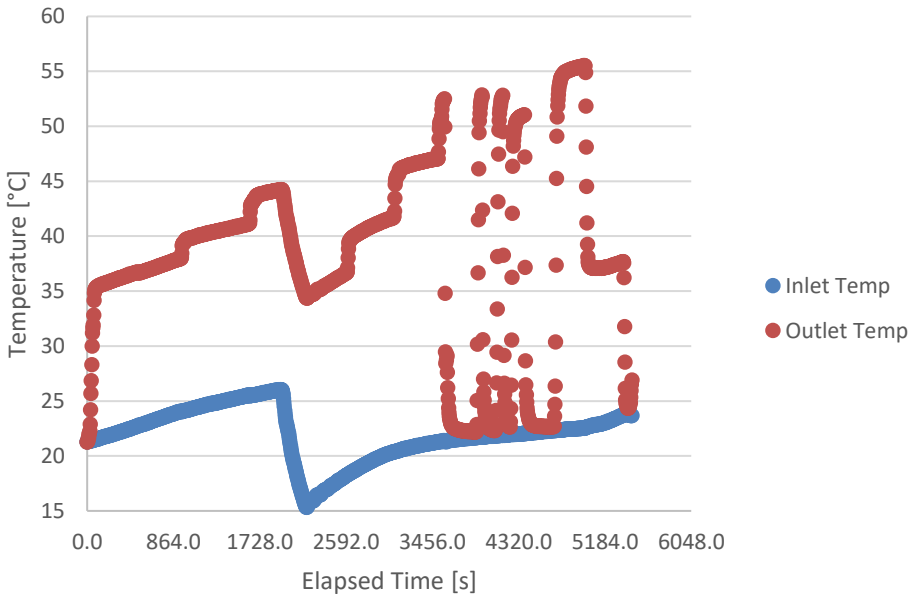

Figure 13 – Transient inlet and outlet helium temperatures for the straight pipe configuration

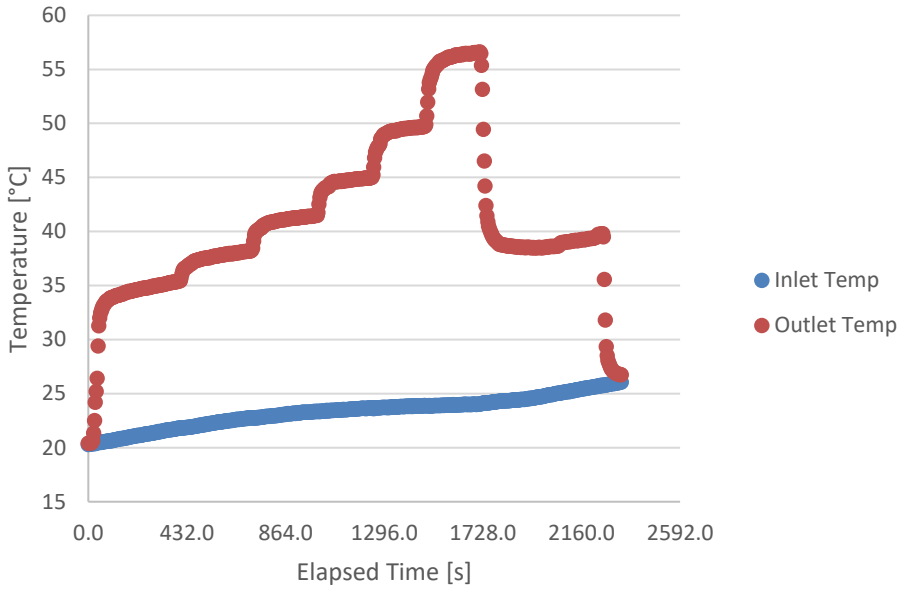

Figure 14 – Transient inlet and outlet helium temperatures for the 90° pipe configuration

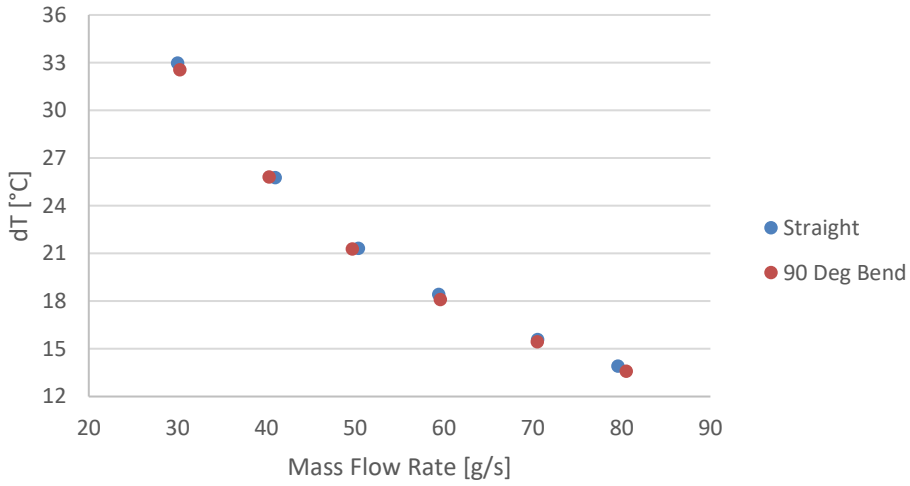

Figure 15 – Helium temperature change upstream and downstream of heaters for both configurations

Individual heater temperatures were measured for both experiments. At first, it was desired to see if any wall flow effects were present on the outer heaters. However, since the heater electrical resistance varied randomly from 62.4 to 67.8 ohms at room temperature, shown in Fig. 16, the individual heater power varied by as much as 8%. This variation in heater power made it impossible to determine small variations in the individual heater temperature based on flow effects. Figures 17 through 22 show the change in temperature between the individual heaters and the helium inlet with their respective flow rates and Reynolds numbers. The heater temperatures for the straight and 90° elbow configurations are different due to the variation in helium inlet temperatures. The heaters with higher electrical resistance have lower temperatures than those with lower resistance (Fig. 16). A temperature change of up to 9°C was seen between the heaters, specifically between heaters 1 and 3.

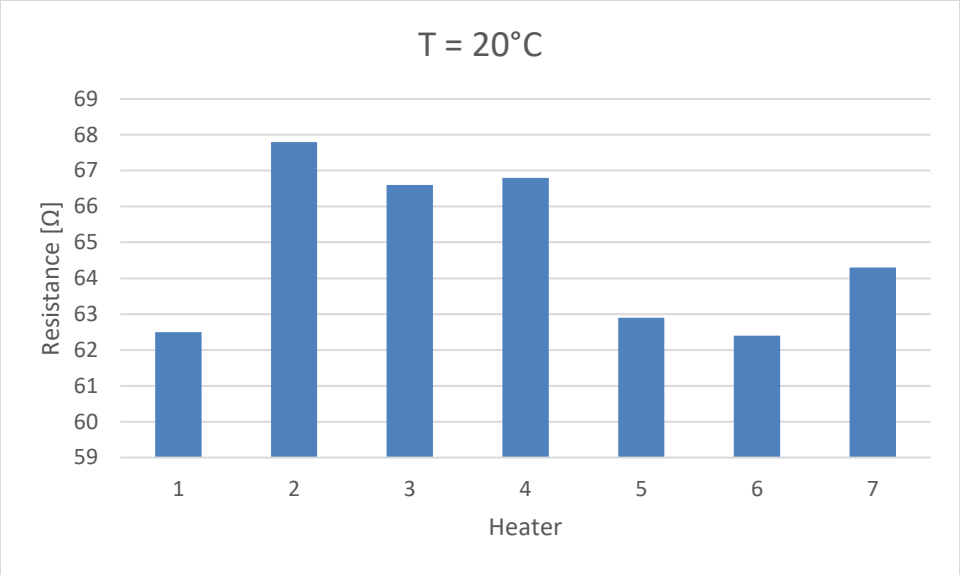

Figure 16 - Heater electrical resistance at 20°C (measured from feedthroughs)

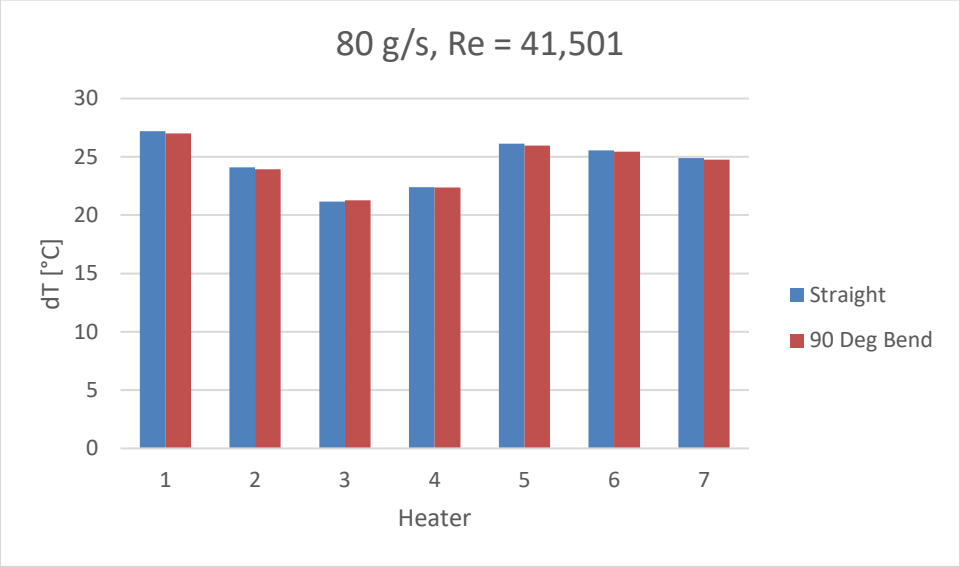

Figure 17 – Temperature change between heaters and helium inlet for the straight and 90° bend configurations at 80 g/s

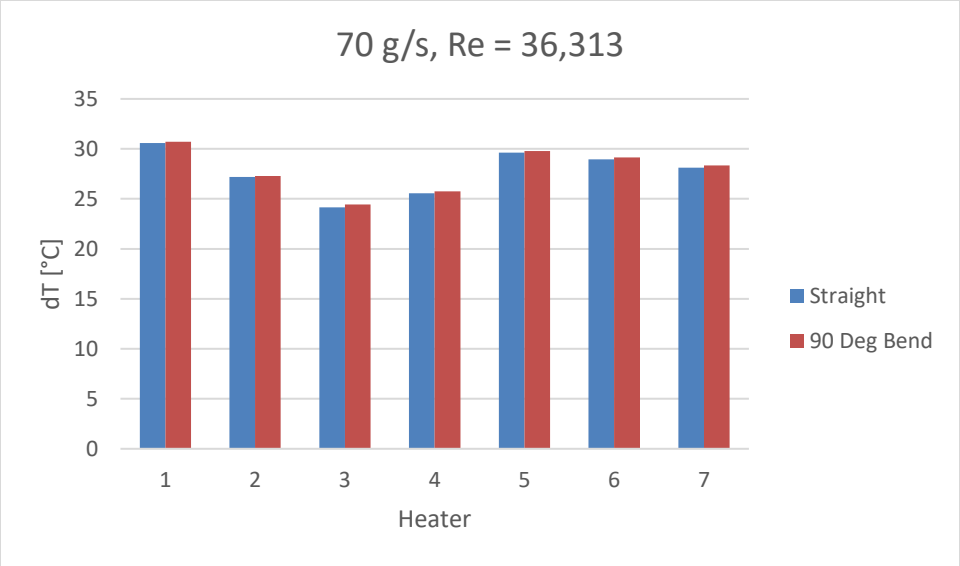

Figure 18 - Temperature change between heaters and helium inlet for the straight and 90° bend configurations at 70 g/s

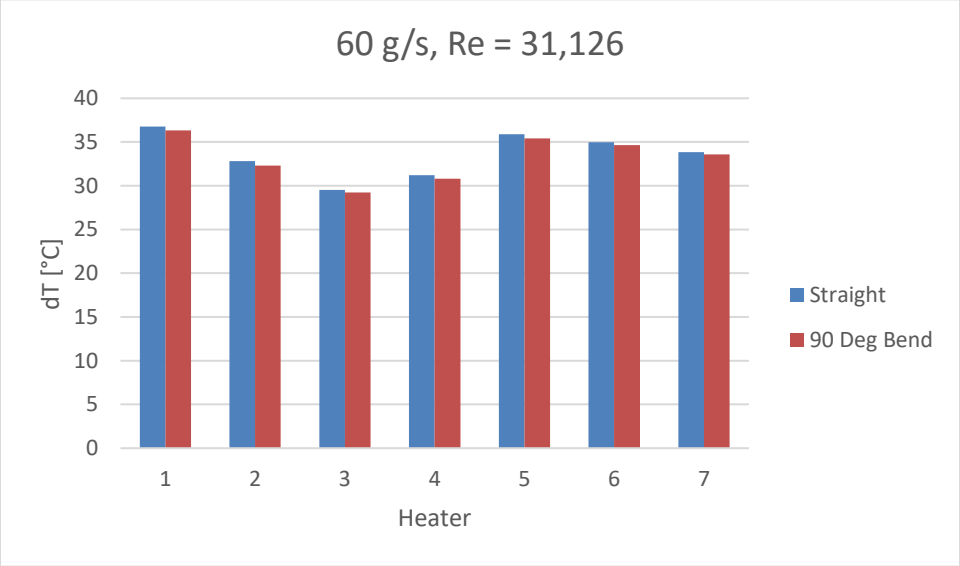

Figure 19 - Temperature change between heaters and helium inlet for the straight and 90° bend configurations at 60 g/s

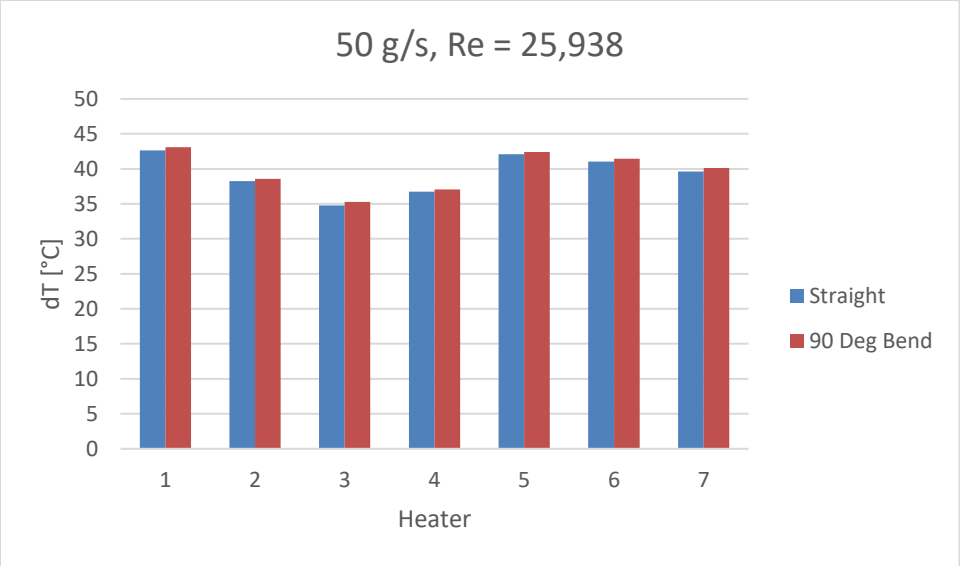

Figure 20 - Temperature change between heaters and helium inlet for the straight and 90° bend configurations at 50 g/s

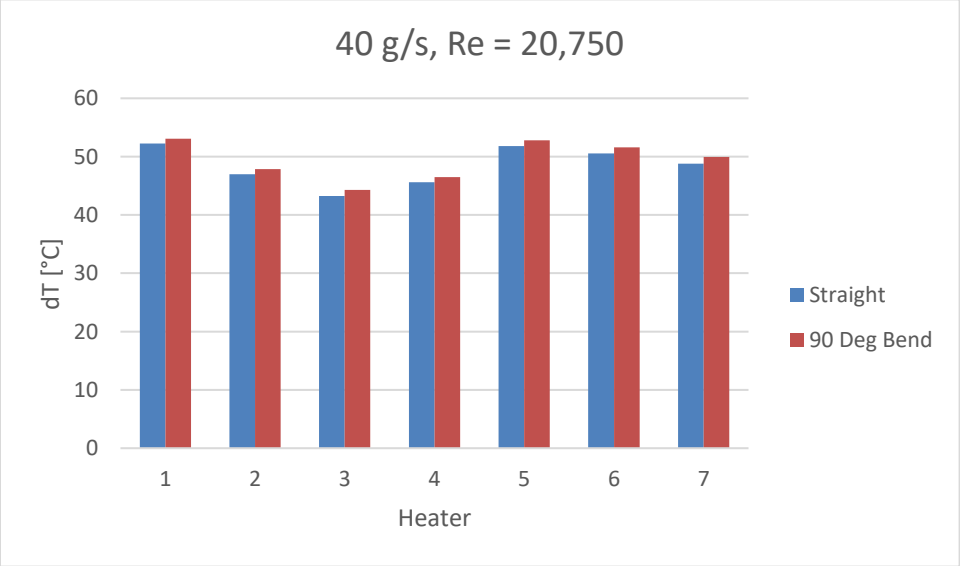

Figure 21 - Temperature change between heaters and helium inlet for the straight and 90° bend configurations at 40 g/s

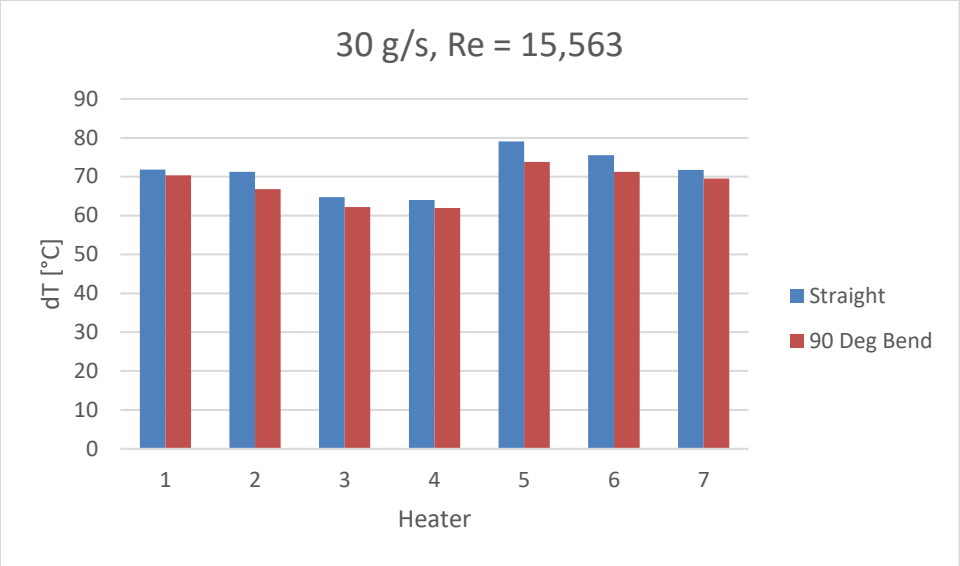

Figure 22 - Temperature change between heaters and helium inlet for the straight and 90° bend configurations at 30 g/s

Simulation

Theory

The convection heat transfer coefficient (HTC) of the helium cooling fluid as well as other flow characteristics can be determined analytically using several fundamental fluid equations. First, the Reynolds number is used to characterize fluid flow as laminar, turbulent, or in a transition state. The Reynolds number for fluid flow in a closed channel is calculated by Eq. 1,

$$Re = \frac{\rho D_h V}{\mu} \tag{1}$$

where D is the inner pipe diameter, V is the mean fluid velocity, and μ is the dynamic viscosity of the fluid. The helium density and viscosity were determined at the mean fluid temperature according to the experiment results. The convective HTC is determined using Eq. 2,

$$h = \frac{Nu\ k}{D_h} \tag{2}$$

where k is the thermal conductivity of the fluid, D_h is the hydraulic diameter of the channel, and Nu is the Nusselt number. The Nusselt number can be expressed using the Dittus-Boelter[1] correlation for heating of a fluid:

$$Nu = 0.0243 Re^{4/5} Pr^{0.4} \tag{3}$$

[1] Incropera and DeWitt, Fundamentals of Heat and Mass Transfer, 7th Ed., Wiley, 2012, p. 544.

where $0 \leq Pr \leq 160$, $Re \geq 10{,}000$, and $\frac{L}{D} \geq 10$. The Nusselt number can also be expressed using the Gnielinski[2] correlation which is valid for smooth tubes over a larger range of Reynolds numbers and is shown in Eq. 4,

$$Nu_D = \frac{(f/8)(Re_D - 1000)Pr}{1 + 12.7(f/8)^{1/2}\left(Pr^{2/3} - 1\right)} \tag{4}$$

where $0.5 \leq Pr \leq 2000$ and $3000 \leq Re \leq 5E6$. The friction factor for smooth tubes is determined by Eq. 5.

$$f = (0.79\ln(Re) - 1.64)^{-2} \tag{5}$$

Pressure drop across the heaters with a bull nose entrance and exit was also determined analytically. The general equation for pressure change in terms of head loss can be seen in Eq. 6,

$$\Delta P = h_f \rho g \tag{6}$$

where h_f is the dynamic head for internal flow. In this experiment, the dynamic head of the flow channels in between the resistive heaters can be determined by Eq. 7,

$$h_f = \left(\frac{fL}{d_h} + \Sigma K\right)\frac{V^2}{2g} \tag{7}$$

where: ΣK is the sum of loss coefficients for the bull nose entrance and exit (0.05 and 0.5, respectively). The friction factor under turbulent conditions for various surface roughness is calculated using Eq. 8,

$$f = \left\{-1.8log\left[\frac{6.9}{Re} + \left(\frac{\frac{\varepsilon}{d}}{3.7}\right)^{1.11}\right]\right\}^{-2} \tag{8}$$

where: ε is the surface roughness of the material (m). Using these correlations, the heater wall temperature is determined by the basic convection heat transfer equation,

$$T_s = T_m + \frac{q"}{h} \tag{9}$$

where T_m is the mean fluid temperature and q" is the wall heat flux (W/m^2). Also, the surface temperature can be related to the maximum heater internal temperature, assuming that both sides are equal temperatures,

$$T_{max} = \frac{\dot{q}L^2}{2k} + T_s \tag{10}$$

where $\dot{q}$ is the internal heat generation of the heater (W/m^3), L is the length from the heater midline to the heater surface, and k is the heater thermal conductivity. In this case, the aluminum nitride heaters have a thermal conductivity of 150 W/m-K.

[2] Incropera and DeWitt, Fundamentals of Heat and Mass Transfer, 7th Ed., Wiley, 2012, p. 545.

CFD

Three dimensional, steady state fluid flow through the array of resistive heaters was modeled using ANSYS Fluent 18.2. Figure 23 shows a cross sectional view of the 3-D heater flow geometry shown in blue. A heat flux boundary condition of 61.9 W/cm^2 was applied to each heater surface to replicate the experimental result. Pressure conditions (340 psig inlet) were applied at the inlet and outlet, and the mass flow rate was determined via the solver. The temperature dependent properties of helium used in this model were viscosity and thermal conductivity from Peterson[3]. Density was solved using the ideal gas law. Since the flow between the heaters is turbulent, even at a low flow rate of 30 g/s, the turbulent k-omega SST model was used in this study. Figure 24 shows a close-up view of the mesh at the bullnose entrance and contains 9,605,628 nodes and 9,254,480 hexahedron and tetrahedron elements. Appropriate inflation layers were set at the walls to accommodate for the boundary layer thickness of the fluid.

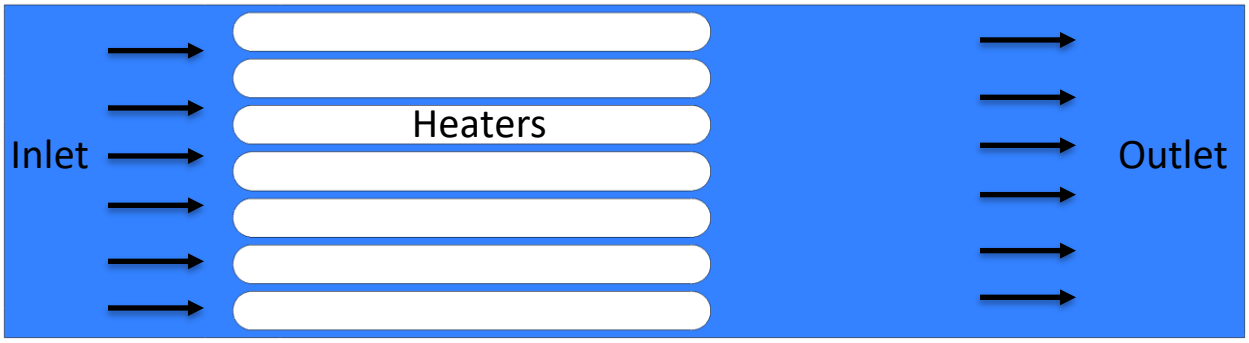

Figure 23 – Cross sectional view of 3-D heater flow geometry in ANSYS Fluent

[3] Peterson, H. (1970). The Properties of Helium: Density, Specific Heats, Viscosity, and Thermal Conductivity at Pressures from 1 to 100 bar and from Room Temperature to about 1800 K. (Danish Atomic Energy Commission, Report No. 224)

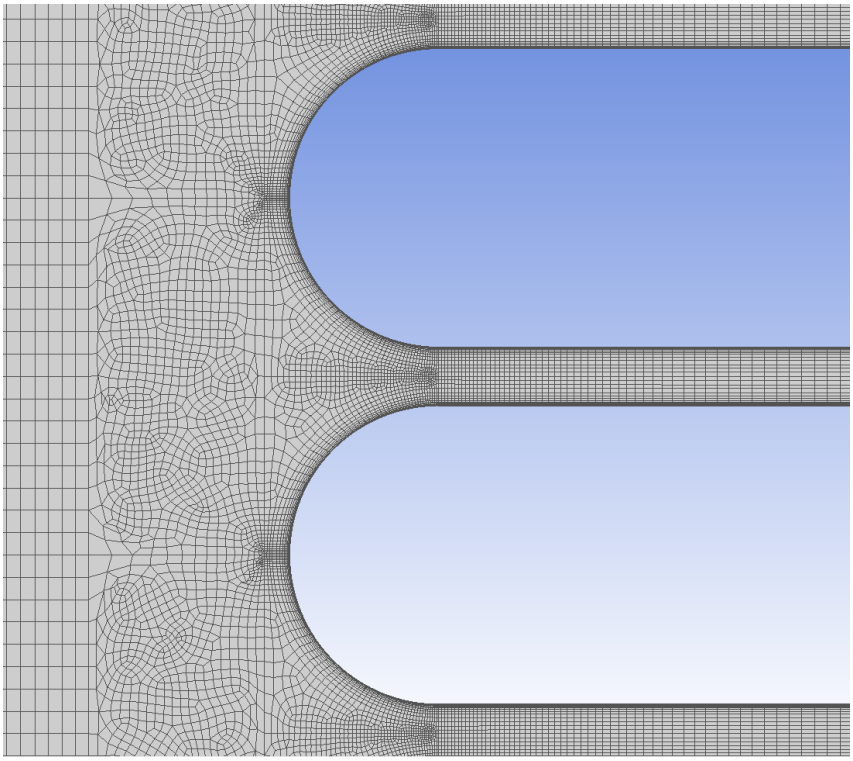

Figure 24 - Close-up view of the mesh cross section at the bullnose inlet

Results

The simulation results were compared to the experimental and analytical results. First, pressure drop as a function of mass flow rate is shown in Fig. 25. The analytical results using the friction factor for smooth tubes (Eq. 5) and the general friction factor correlation (Eq. 8) are also included. One can see that the pressure drop using the general friction factor correlation matches closely with the experimental results. However, the pressure drop was measured throughout the entire He flow loop and not just the heater test section. Therefore, the actual pressure drop should be slightly less than what is shown in this plot. Also, the CFD result slightly overestimates the pressure drop across the heaters.

The analytical, CFD, and experimentally determined average heater surface temperatures are shown in Fig. 26. Since the heater temperature from the experiment was measured at the center of each heater, Eq. 10 can be used to estimate the average surface temperature. It is shown that the estimated experimental heater surface temperature is less than the CFD results, the Dittus-Boelter, and the Gnielinski correlations. However, around a flow rate of 30 g/s, the surface temperature using the Dittus-Boelter correlation shows a close match with the CFD results. Temperature differences between experiment and CFD results range from approximately 30°C at 30 g/s, to about 10°C at 80 g/s. Temperature differences between experiment and the Dittus-Boelter correlation results range from approximately 32°C at 30 g/s, to about 22°C at 80 g/s. The calculated surface temperatures from the Gnielinski equation are about 5-10°C greater than determined using the Dittus-Boelter correlation.

The average heat transfer coefficient between the heaters at various mass flow rates is shown in Fig. 27. The experimentally determined HTC values (straight and 90° bend geometries) are determined from Eq. 9 using the estimated surface temperatures described earlier. Again, the experimental values are compared to analytical calculations and CFD results. One can see how large the experimental HTC is compared to the analytical and CFD results. The experimentally determined HTC at a flow rate between

30 to 80 g/s is 46-153% greater than the Dittus-Boelter correlation, respectively. The expected HTC at 80 g/s using the Dittus-Boelter correlation is 16,741 W/m^2-K, whereas the experimentally determined HTC is about 42,500 W/m^2-K. Clearly, this is not a realistic value since this would place the HTC in the liquid metal flow range. Several tests were performed to try to diagnose the high HTC results. First, the heater thermocouples were tested in boiling water to verify correct operation. Next, a sticky thermocouple was placed on the heater surface during adiabatic heating to verify higher temperature accuracy. Lastly, the thermal test using the 90° bend geometry was performed a second time with new heaters and a new power supply with similar results.

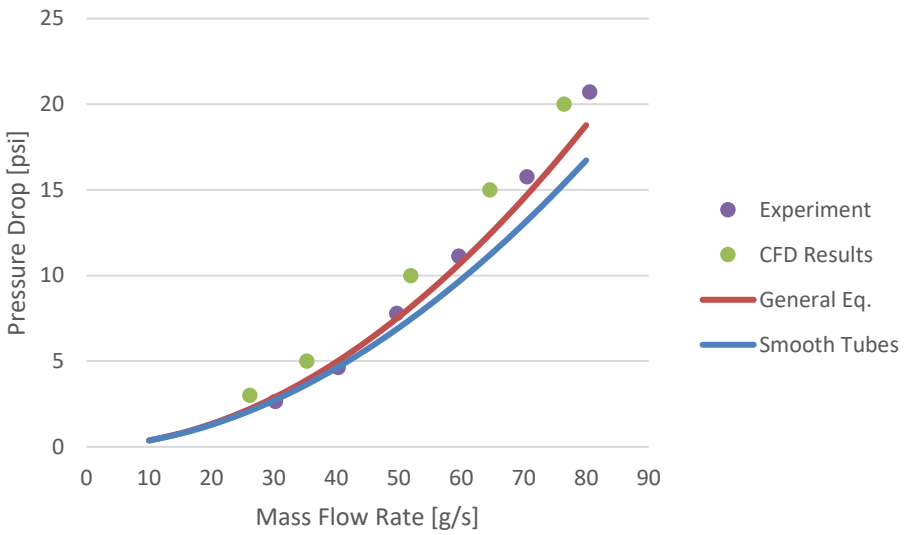

Figure 25 - Pressure drop across resistive heaters in 90° bend configuration (inlet pressure is 340 psig)

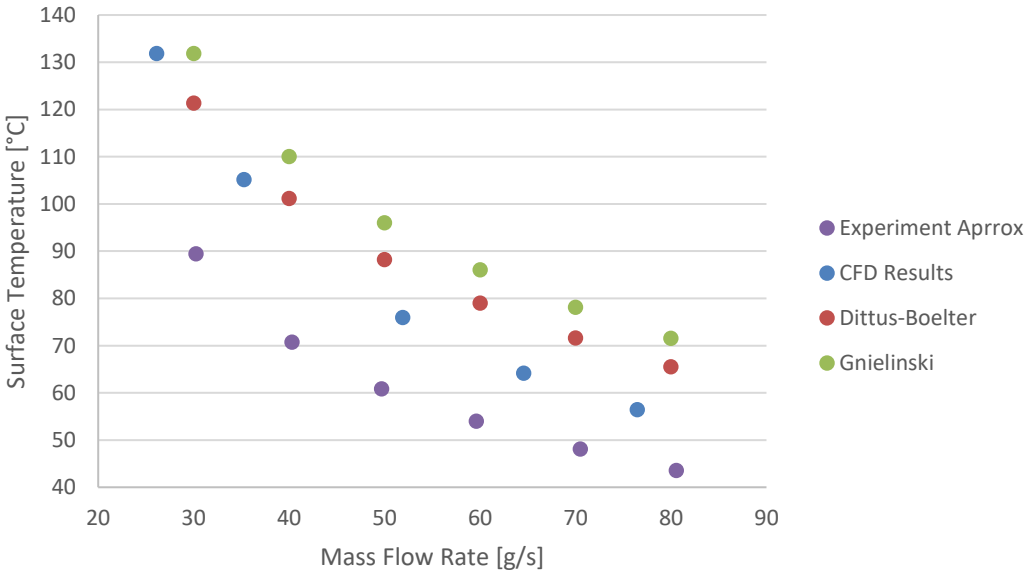

Figure 26 - Heater surface temperature comparison between theory, CFD, and experimental approximations

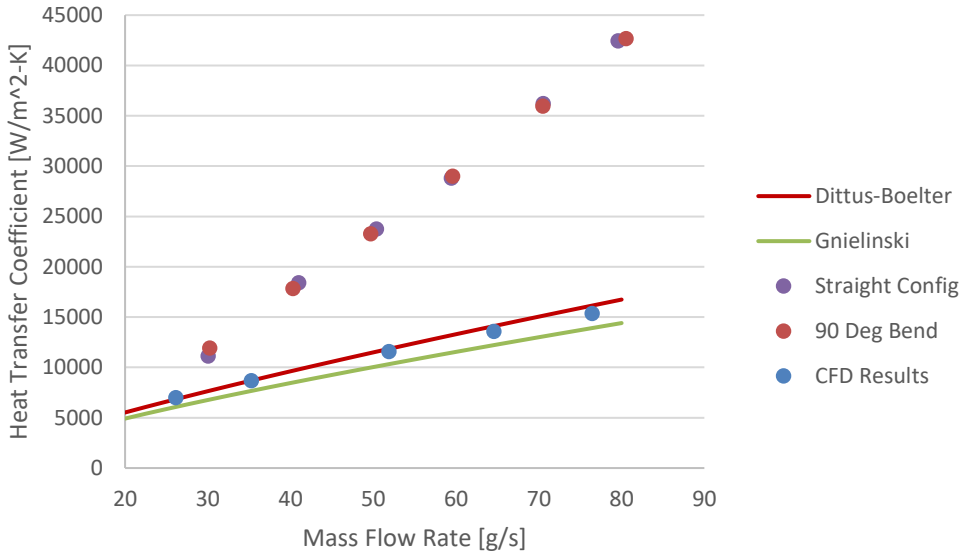

Figure 27 - Heat transfer coefficient comparison between theory, CFD, and experiment

Velocity contour plots of the CFD results for a pressure drop of 5 and 20 psi and a flow rate of 35 g/s and 77 g/s, respectively, is shown in Figs. 28 and 29. Flow separation at the bullnose outlet can be seen in both figures. Also, the array of flow channels appear to create areas of circulation after the bullnose outlet. Flow circulation is typically not desired since it increases pressure losses. Figures 30 and 31 show this circulation in more detail using streamlines as a flow visualization tool. Note that the streamlines within the flow channels are not centered, thus, wide ranges of velocities are shown. One can see that there is a large area of low velocity circulating fluid after the bullnose exit in the 35 g/s case. In the 77 g/s case, the circulation is more sporadic and is circulating parallel to the flow channels.

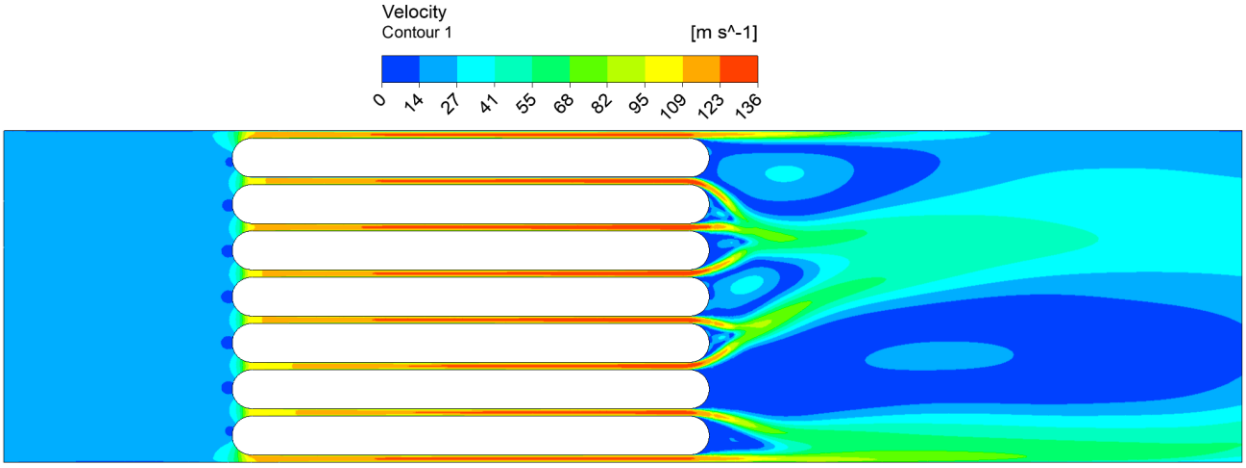

Figure 28 – Velocity contour plot for a 5 psi pressure drop, mass flow = 35 g/s, Re = 22,187

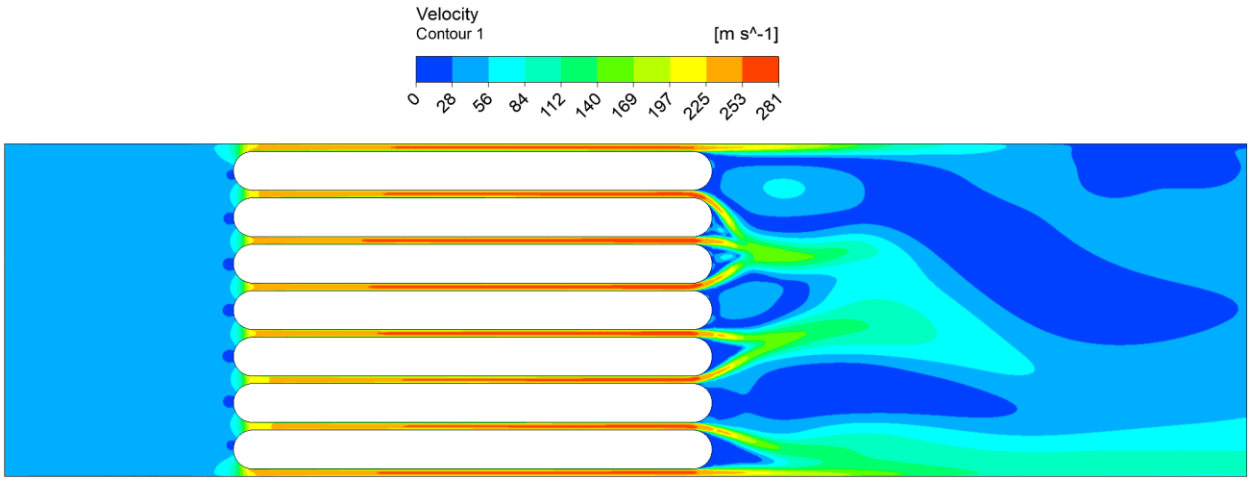

Figure 29 - Velocity contour plot for a 20 psi pressure drop, mass flow = 76.5 g/s, Re = 47,765

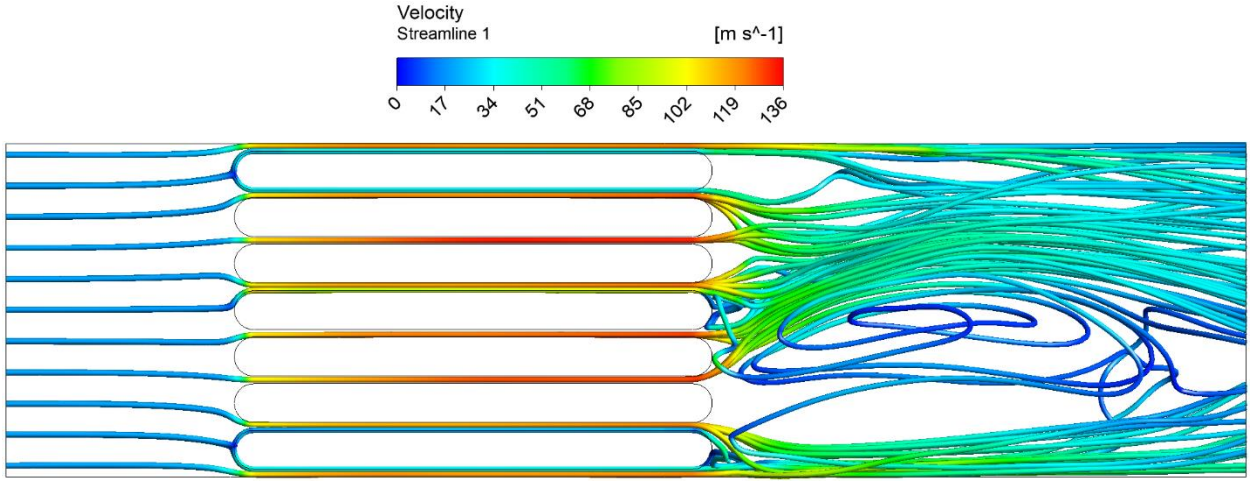

Figure 30 – Streamlines for a 5 psi pressure drop, mass flow = 35 g/s, Re = 22,187

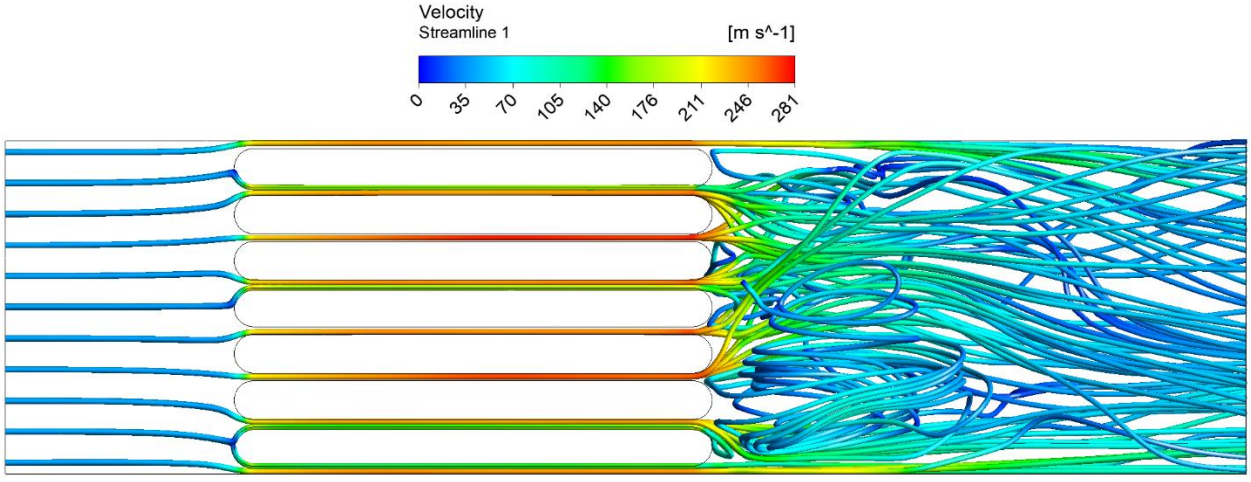

Figure 31 - Streamlines for a 20 psi pressure drop, mass flow = 76.5 g/s, Re = 47,765

Temperature contour plots are shown in Figs. 32 and 33 for mass flow rates of 35 and 77 g/s, respectively. For the 77 g/s case, the helium temperature actually decreases as it passes through the bullnose inlet, and then gradually increases from the heaters. The temperatures at the outer walls near heaters one and seven have minimal increase since there is no heating occurring at that surface. There is also some localized high temperatures in low velocity regions where boundary layer separation occurs at the bullnose outlet.

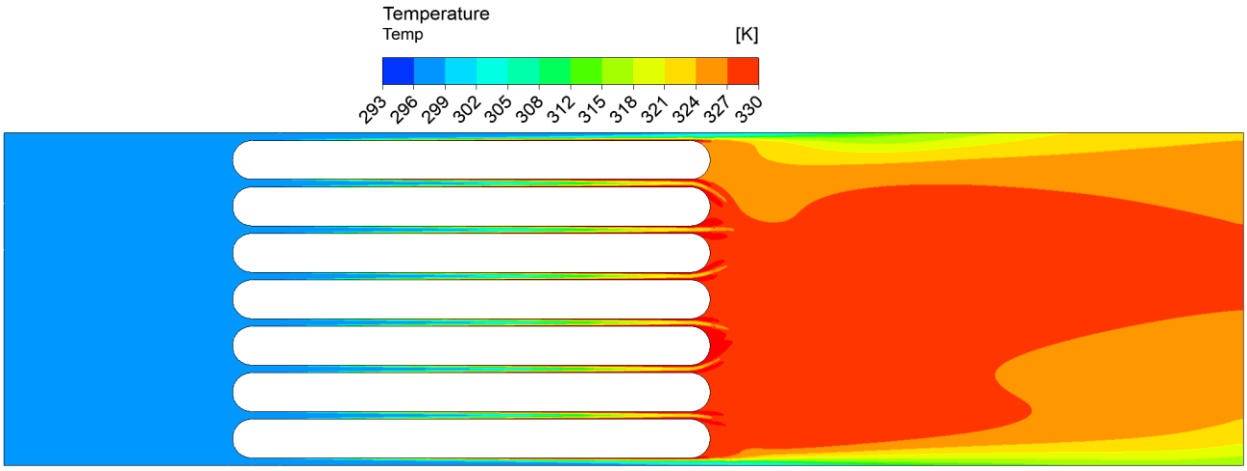

Figure 32 - Temperature contour plot for a 5 psi pressure drop, mass flow = 35 g/s, Re = 22,187

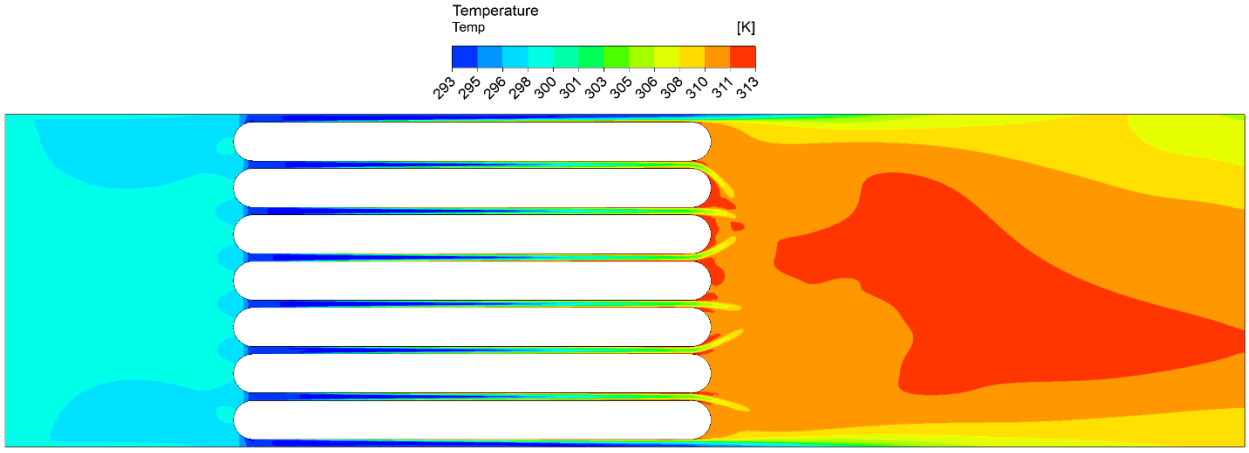

Figure 33 - Temperature contour plot for a 20 psi pressure drop, mass flow = 76.5 g/s, Re = 47,765

Conclusion

Three successful heater experiments were conducted using the straight and 90° bend pipe configurations. As expected, the production facility, 90° bend pipe configuration restricted helium flow slightly more than the straight, fully developed flow configuration. However, the pressure loss between the two configurations was small and only within one psi of one another at 80 g/s. The resistive heaters performed as expected, however, since each heater had a different electrical resistance, individual power and temperature varied widely. Nonetheless, total power and average heater temperature provided valuable information for comparisons between the CFD and analytical results.

Pressure loss from the resistive heaters showed good agreement with CFD and theory. However, surface heater temperature varied widely between the experiment, CFD and theory. Up to a

42°C temperature difference at 30 g/s was seen from experiment results to theory, and a temperature difference of 30°C at 30 g/s compared to CFD. At 80 g/s, the results were much closer to the experiment. A temperature difference of 10°C from the CFD results and 28°C from theory were determined. Additional tests need to be performed to diagnose the high temperature differences. All in all, the resistive heater experiments were performed successfully, yet additional questions remain unanswered and should be investigated in future work.

Future Studies

Another set of experiments using the resistive heater assembly will be performed with slight modifications and configuration changes. First, it will be very useful to understand the fluid and thermal behavior if a Mo-100 plant design disk were to break during heating. Assuming the disk gets ejected out of the holder, a large gap would form between adjacent disks, creating a low velocity region that decreases disk cooling ability. Therefore, a similar series of experiments will be performed with one heater removed to determine the flow and thermal effects on the heater assembly. Also, if a flow channel were to get blocked by debris, studying the resulting flow behavior will be very beneficial for understanding how to prepare for such an unexpected scenario.

Appendix A

Power breakout box electrical circuit